Kovove Mater. 52 2014 149–155
DOI: 10.4149/km_2014_3_149

Corrosion behaviour of Fe-40Al-Zr (at.%) alloy in molten soda-lime glass

A. Hotař[1]*, V. Hotař[2], F. Novotný[3]

[1] *Technical University of Liberec, Faculty of Engineering, Department of Material Science, Studentská 2, 461 17 Liberec, Czech Republic*
[2] *Technical University of Liberec, Faculty of Engineering, Department of Glass Producing Machines and Robotics, Studentská 2, 461 17 Liberec, Czech Republic*
[3] *Institute of Chemical Technology, Department of Glass and Ceramics, Technická 5, 166 28 Prague 6, Czech Republic*

Received 11 December 2013, received in revised form 29 January 2014, accepted 12 February 2014

Abstract

The corrosion behaviour of Fe-40Al-Zr (at.%) has been investigated in molten soda-lime glass at 1200 °C. The measurement of weight loss and surface change were used for explanation of the corrosion resistance. The alloying by 0.09 at.% Zr reduces the corrosion resistance of Fe-40Al-Zr against molten soda-lime glass in comparison with earlier tested Fe-25Al-5Cr alloy. The corrosion mechanism of Fe-40Al-Zr alloy in molten soda-lime glass was also described. During reactions between tested iron aluminide and glass oxides, Al_2O_3 was generated and preferential oxidation of Zr-rich precipitates occurred.

K e y w o r d s: iron aluminide (FeAl type), corrosion behaviour, molten soda-lime glass

1. Introduction

Fe-Al and Fe_3Al based alloys are of interest as possible replacement for various stainless steels because their high-temperature oxidation resistance is very good [1–3]. Other advantages of Fe-Al and Fe_3Al based alloys are low material cost and their low density compared to that of steels. However, high-temperature strength and creep properties of binary Fe-Al alloys are insufficient for structural applications. One of the ways to improve strength at high-temperature is alloying by elements, which cause formation of second phases as strengthening particles (for example Zr, Nb or Ta), or solid solution strengthening (for example Ti) [4–7].

Iron aluminides are generally regarded as very oxidation resistant because dense and adherent oxide scales of α-Al_2O_3 form on the surface [1–3]. However, the phase composition of scales can change depending on the chemical composition of the alloy, temperature and exposure time. In addition to α-Al_2O_3, scales can also contain metastable γ-, δ-, θ-Al_2O_3 and iron oxides and oxides of ternary alloying elements, which cause an increase of the oxidation rate in many cases. The Zr content influences the oxidation behaviour of Fe_3Al alloys very significantly. The positive effect of small Zr concentrations on the oxidation behaviour of Fe_3Al alloys was already discussed [2, 8–10]. The addition of Zr in the range 0.05–0.1 at.% is used as reactive element, which improves especially the adherence of the α-Al_2O_3 scales on the Fe_3Al-Cr alloys [8, 10, 11]. If the Fe_3Al-Cr alloy's content of Zr is in the range 0.1–1.0 at.%, very good oxidation resistance was observed only up to 900 °C [12, 13]. The temperature increase above 1000 °C causes the penetration of oxides into the samples what increases the oxidation rate [12, 13]. Large amounts of Zr (above 1 at.%) have detrimental effect on the oxidation behaviour even at 900 °C [6].

Testing of the corrosion resistance against molten glasses has been stimulated by the very good oxidation resistance of iron aluminides in air. First test of alloys based on Fe-Al (with 40–45 at.% Al) in the glass industry was performed by Uxa [14] in the early fifties of the 20th century. This alloy was used specifically for burners, valves, holders, etc., and replaced the elements from cast iron. The corrosion resistance of iron

*Corresponding author: tel.: +420 485 353 136; e-mail address: adam.hotar@tul.cz

Table 1. Chemical composition of the alloys in at.%

Alloy	Al	Cr	Zr	Mn	B	Mo	Fe
Fe-40Al-Zr	40.61	0.02	0.09	0.15	0.05	0.01	Bal.

aluminides based on Fe_3Al type alloys against soda-lime glass and molten lead crystal was reported in [15, 16]. The results were compared with austenitic steel (EN X8CrNi25-21), which is frequently used in molten glasses.

It is the purpose of this paper to present corrosion tests of Fe-40Al-Zr (at.%) in molten soda-lime glass. The findings extend the knowledge about corrosion resistance and behaviour of iron aluminides in molten soda-lime glass, which is used for the production of flat and container glass.

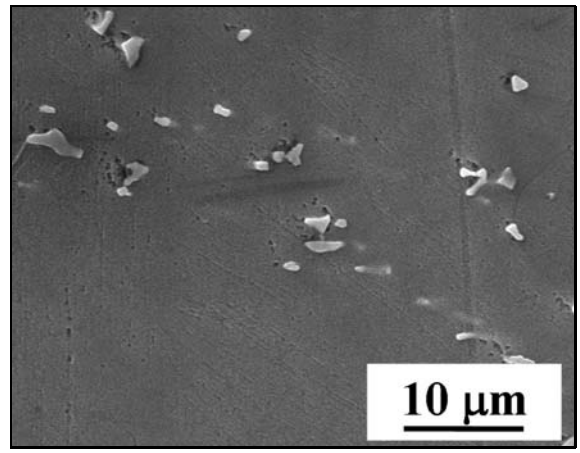

Fig. 1. SEM-SE micrograph of Fe-40Al-Zr alloy in the as rolled condition; detail of ZrC particles (light phase) in FeAl matrix (dark gray).

2. Experimental

The composition of the tested material is given in Table 1. The alloy contained also carbon as technical impurity coming from the raw metal, which was used for the preparation of the alloys. A vacuum induction furnace was used for melting of the alloy. The ingot (approximately 19 mm × 33 mm in cross section) was subsequently hot rolled at 1200 °C in ten passes to a sheet of 5.3 mm thickness. Rolling of the ingot was performed in a protective capsule as described in [17]. Small cuboids were cut from the sheet and the sample surfaces were ground using SiC papers up to 1200 grit.

The corrosion experiments were performed in soda-lime glass (Table 2) at 1200 °C. Each sample was placed (on the smallest side of cuboid) in an alumina crucible and the crucible was subsequently filled with glass scrap. Then the crucible was heated to 1200 °C in a muffle furnace. The corrosion tests were carried out for 24, 48, 72 and 96 h. After each time interval, the crucible was cooled down slowly in the furnace. The cold crucible was carefully broken and the glass separated from the surface of the samples. The corrosion behaviour in molten glass was investigated by measuring the weight loss and the change of surface roughness. For each time interval, weight loss is an arithmetic average of three measurements. Chemical analysis of the samples surface was carried out by energy-dispersive X-ray spectrometry (EDS; Bruker). For the determination of the chemical composition of the glass, an ARL 9400 XP sequential WD-XRF spectrometer was used.

3. Results and discussion

The microstructure of Fe-40Al-Zr alloy consists of FeAl matrix and ZrC particles after hot rolling at 1200 °C. The phase analysis has been performed by EDS (Fig. 1).

The behaviour of Fe-40Al-Zr alloy in contact with molten soda-lime glass was determined by measurements of mass loss, roughness change and chemical analysis of samples surface and glass. Figure 2 reveals the corrosion kinetics of the tested alloy in molten soda-lime glass at 1200 °C. The slope of the curves shows that Fe-40Al-Zr dissolves faster in the early stage. The slowing down of solution of Fe-40Al-Zr after 72 and 96 h of interaction is probably caused by an increased concentration of corrosion products (probably iron disilicide or oxides of the alloy) near the surface of samples. This saturated area presumably partially reduces chemical reaction between the alloy and the molten glass. However, the corrosion rate of Fe-40Al-Zr in molten soda-lime glass is the highest

Table 2. Chemical composition of soda-lime glass determined using XRF analysis

Composition (wt.%)	SiO_2	Al_2O_3	Fe_2O_3	CaO	MgO	K_2O	Na_2O	SO_3	TiO_2
Before corrosion test	72.359	0.982	0.087	8.411	4.237	0.221	13.426	0.121	0.063
After corrosion test at 1200 °C/96 h	71.587	1.234	0.098	8.407	4.388	0.209	13.707	0.231	0.063

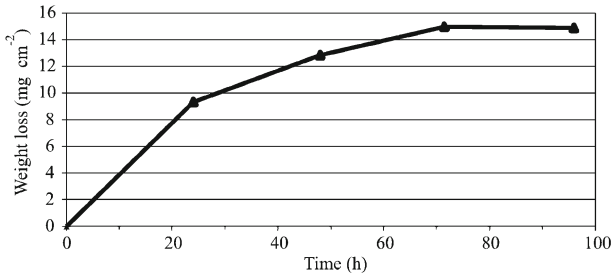

Fig. 2. Weight loss of Fe-40Al-Zr as a function of time during interaction with soda-lime glass at 1200 °C.

Table 3. Corrosion rates of iron aluminides in soda-lime glass at 1200 °C, calculated from weight loss after 96 h

Alloys	Corrosion rates (mm/year)	Reference
Fe-40Al-Zr	2.1	This work
Fe-28Al-3Cr-0.5Zr*	x	[16]
Fe-25Al-5Cr	1.4	[16]
EN X8CrNi25-21	1.8	[16]

*weight gain was measured

among the compared iron aluminides (Table 3). Iron aluminides and steel from [16] were tested in different molten soda-lime glass (container glass instead of flat glass), but the composition of both glasses is very similar, therefore it is possible to compare the corrosion rates.

Corrosion rate R was evaluated from

$$R = 87.6\frac{W}{ATd}, \tag{1}$$

where W is the weight loss (mg), A is the area of a sample (cm^2), T is time of exposure (h) and d is the density of alloy (g cm^{-3}).

The corrosion resistance of the tested alloy may be described also using the roughness of the surface. The surface roughness of samples was measured after 96 h exposure to molten glass. The cross section of the surface was investigated using light optical microscopy, see Fig. 3a. The shape of the surface – dividing line between the alloy and glass (boundary curve) was evaluated (Fig. 3b) and described by image analysis using a software tool developed in Matlab [18]. Many types of parameters can be used for a quantification of the metal roughness. The parameters can be divided into three groups:

(i) *parameters of amplitude,* useful for corrosion depth characterization, Rt – maximum roughness is used as an example in Table 4 (Fig. 3c), the parameter is surface profile parameter defined by standard ISO 4287-1997;

(ii) *parameters of frequency,* used to describe surface profile spacing parameters and for corrugation frequency characterization, an example in the Table 4 is Sm – mean spacing used (Fig. 3c), the parameter is defined by equation:

$$\mathrm{Sm} = \frac{1}{n}\sum_{i=1}^{n} S_i; \tag{2}$$

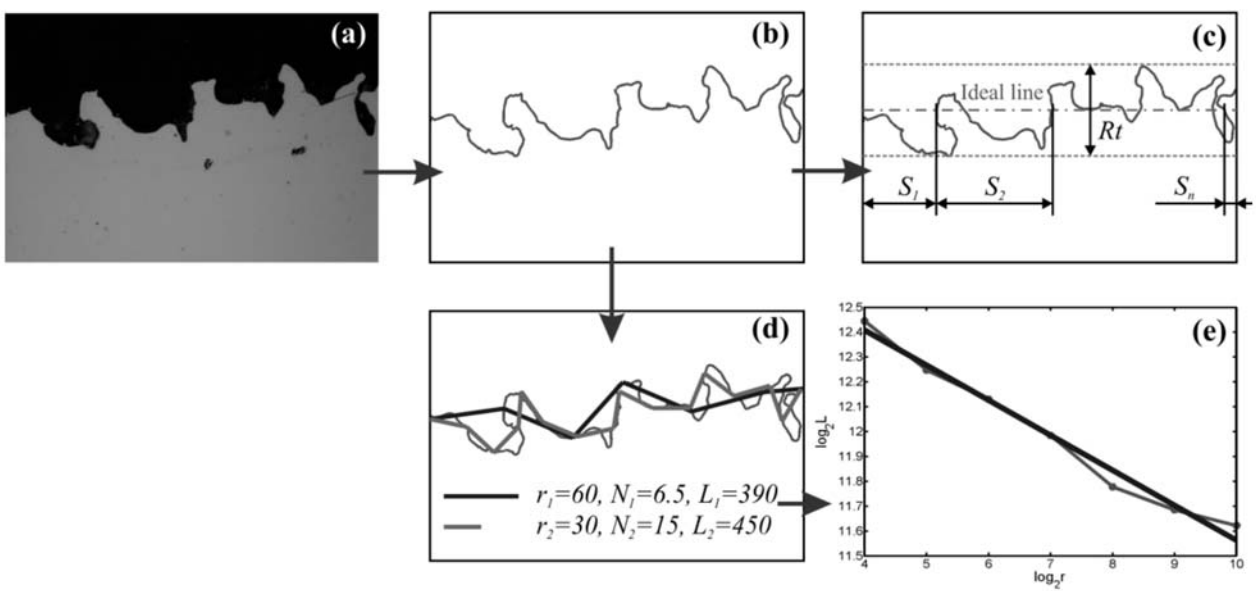

Fig. 3. Image analysis: gray scale image from light optical microscopy (a), evaluated dividing line between the alloy and glass (boundary curve) (b), parameter of amplitude (Rt – maximum roughness) and parameter of frequency (Sm – mean spacing) (c), computing of compass dimension: measurement of profile length by different ruler r_i (d), generation of Richardson-Mandelbrot plot, a compass dimension computing D_C from slope (e).

Table 4. The roughness parameters of boundary curves of alloys after corrosion test at 1200 °C/96 h

Parameters (average of ten measured sections)	Fe-40Al-Zr	Fe-28Al-3Cr-0.5Zr	Fe-25Al-5Cr	EN X8CrNi25-21
Rt – Maximum roughness (μm)	36.0	127.7	8.1	28.4
Sm – Mean spacing (μm)	38.5	25.6	14.6	18.4
D_C 1000 – Compass dimension, estimated Fractal dimension (–)	1072	1203	1017	1090

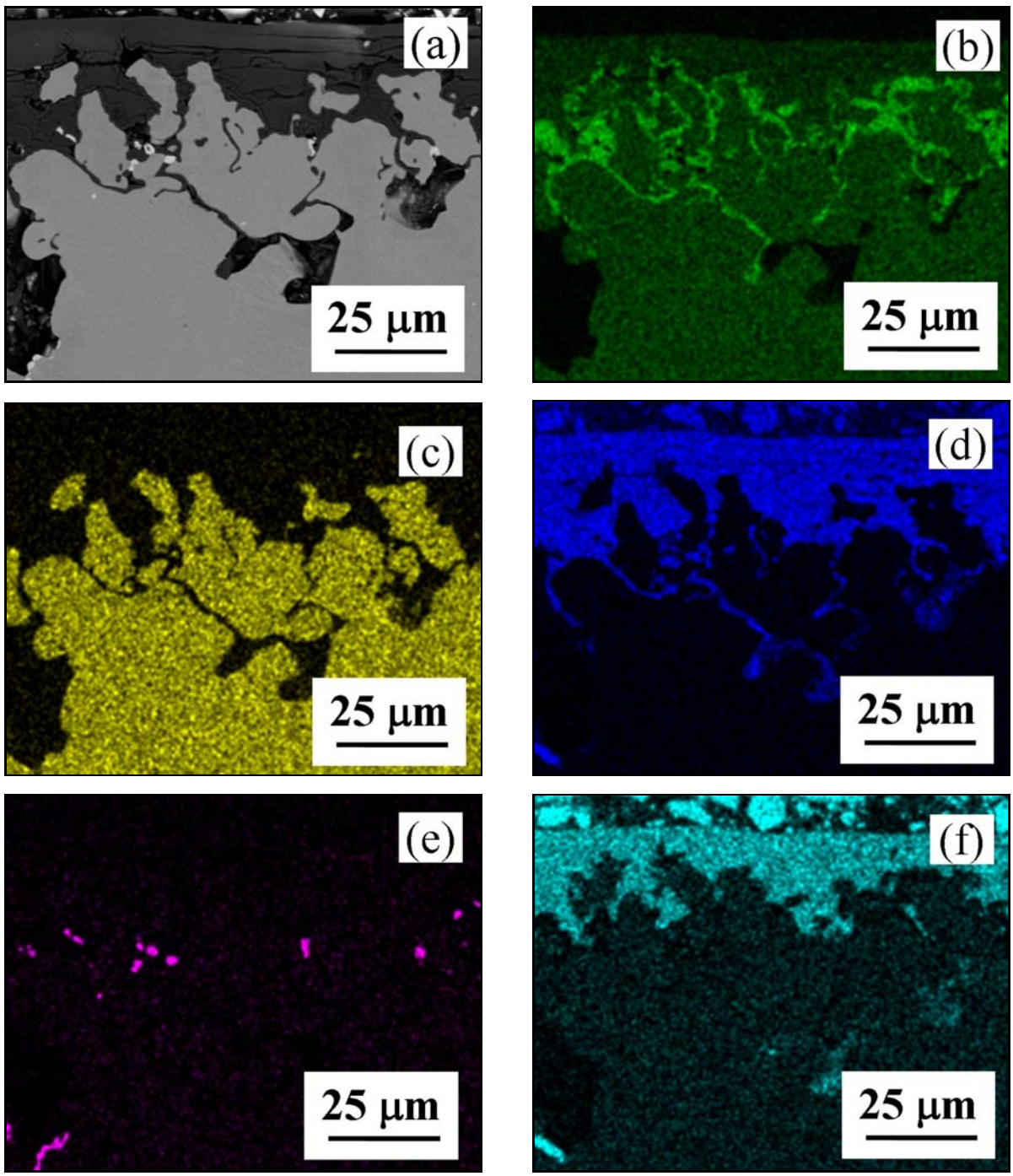

Fig. 4. The cross section of glass/metal interface after interaction Fe-40Al-Zr (at.%) with soda-lime glass at 1200 °C/96 h, SEM-BSE micrograph (a) and mappings of elements: Al (b), Fe (c), O (d), Zr (e) and Si (f).

(iii) *parameters of complexity and deformation,* estimating of fractal dimension by compass dimension (D_C).

The estimated compass dimension expresses the degree of complexity of the interface between alloy and glass by means of a single number [19]. A compass method [19, 20] is based on measuring the dividing line (roughness profile) using different sizes of rulers (Fig. 3d) according to the equation:

$$L_i(r_i) = N_i(r_i) \cdot r_i, \tag{3}$$

where L_i is the length in i-th step of the measurement, r_i is the ruler size and N_i is the number of steps needed for the measurement that is given by the power law:

$$N(r_i) = \text{const} \cdot r_i^{-D_C}. \tag{4}$$

If the line is fractal and hence the estimated fractal dimension is larger than the topological dimension, the length measured increases as the ruler size is reduced. Using previously mentioned equations it will be obtained

$$L_i(r_i) = N_i(r_i) r_i = \text{const} \cdot r_i^{-D_C} \cdot r_i = \text{const} \cdot r_i^{1-D_C}, \tag{5}$$

where D_C is the estimated dimension: the compass dimension.

The logarithmic dependence between $\log_2 N(r_i)$ and $\log_2 r_i$ is called the Richardson-Mandelbrot plot (Fig. 3e). The compass dimension is then determined from the slope s of the regression line:

$$D_C = 1 - s = 1 - \frac{\Delta \log_2 L(r)}{\Delta \log_2 r}. \tag{6}$$

The dimension is multiplied by 1000 (D_C 1000). The fractal dimension can be also estimated by the use of many other methods [19, 20].

The roughness parameters of Fe-40Al-Zr were compared with previously tested alloys under the same corrosion conditions (Table 4). The tested material Fe-40Al-Zr has a deeper surface disruption than the austenitic steel and Fe-25Al-5Cr (Rt – maximum roughness). On the other hand, an uneven and very deep penetration of oxygen into the sample was observed in the case of Fe-28Al-3Cr-0.5Zr. The mean spacing parameter shows that the surface of alloy Fe-40Al-Zr has most peaks and holes compared to the ideal line. However, the oxidation proceeds more uniformly (low value of D_C 1000) than austenitic steel and Fe-28Al-3Cr-0.5Zr.

EDS analyses of the glass/metal interface of Fe-40Al-Zr alloy reveal an oxidation behaviour, which is similar to that of iron aluminides based on Fe_3Al [16]. The generation of alumina was the result of reactions between FeAl matrix of tested alloy and glass oxides (especially with SiO_2), see Fig. 4. The generated alumina dissolved in the molten glass (Table 2) in contrast to the oxidation of iron aluminides in air, which is characterized by formation a thin protective layer of Al_2O_3 [1–3]. However, amount of alumina in the molten glass near the sample surface increases during the interaction and the saturated molten glass reduces further reaction between iron aluminide and the molten glass (unsaturated). In addition to alumina, the reaction between FeAl and SiO_2 generates FeSi and Fe_3Si, which are inert. It is assumed that an increased concentration of FeSi and Fe_3Si partially protects the alloy against further dissolution of alloy similarly as alumina.

On the other hand, the presence of Zr-rich particles in Fe-40Al-Zr alloy has detrimental effect on the oxidation rate in soda-lime glass (Table 3). Post mortem investigation of the sample after interaction with the molten glass for 96 h revealed an increased amount of ZrO_2 at the alloy/glass interface (Table 5). The formation of ZrO_2 was caused by the preferential oxidation of zirconium from Zr-rich precipitates during reactions with sulphate ions or other oxides of the glass (for example SiO_2). The preferential oxidation probably caused the non-uniform attack of the sample surface (the greater waviness of the boundary curve), see Fig. 5. Similar preferential oxidation behaviour was observed after oxidation in air [12, 13, 21].

Figure 6 (colour version on the website) shows the

Table 5. Chemical composition of interface alloy/glass, area EDS analyses

Elements	O	Na	Al	Si	S	Fe	Zr
(wt.%)	41.24	0.16	43.39	1.22	1.15	0.74	12.09
(at.%)	58.35	0.16	36.40	0.98	0.81	0.30	3.00

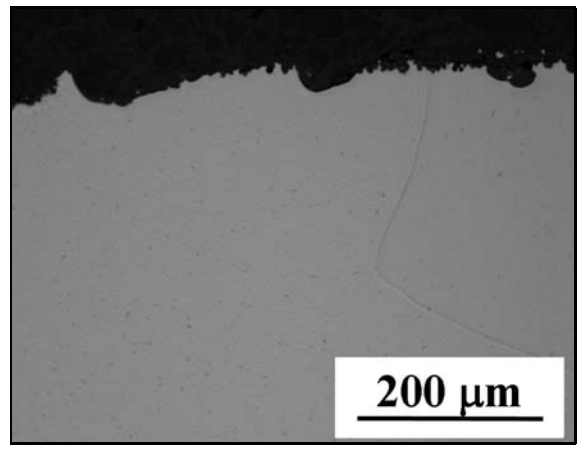

Fig. 5. LOM micrographs of the cross section of Fe-40Al-Zr (at.%) after interaction with soda-lime glass at 1200 °C/96 h.

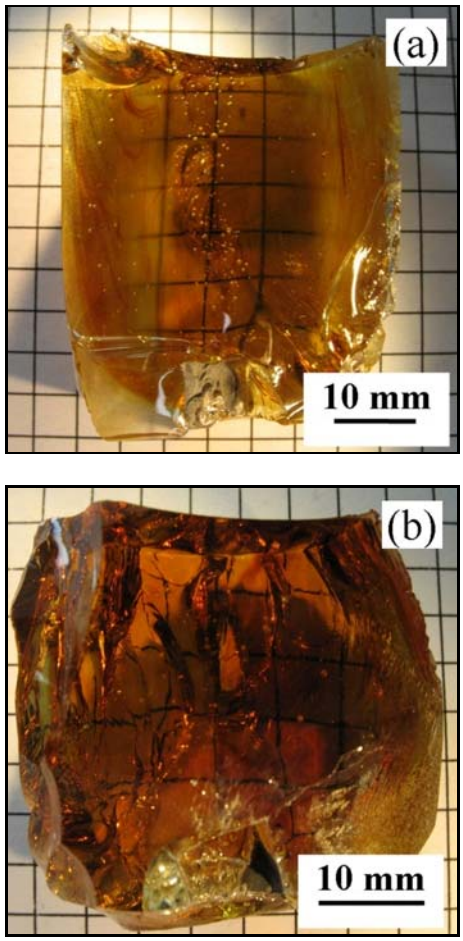

Fig. 6. The tinting of soda-lime glass after interaction with Fe-40Al-Zr (at.%) at 1200 °C after time interval 24 h (a) and 96 h (b).

tinting of the glass after interaction with Fe-40Al-Zr. The yellow-brown tint is caused by the presence of the polysulphide of iron. The polysulphide of iron is a product of the reaction between the sulphate ions and Fe_2O_3, which occurs under reducing conditions. The yellow-brown tint of soda-lime glass due to interaction with iron aluminides was already observed earlier [16]. In case of Fe-40Al-Zr, the soda-lime glass has no grey areas, which were observed in glass after interaction with Fe-28Al-3Cr-0.5Zr or Fe-25Al-5Cr. The grey tinting was caused by a formation of Si small particles.

The interaction between Fe-40Al-Zr and molten soda-lime glass also results in the generation of bubbles (Fig. 6). The bubbles mainly contain SO_2. The source of SO_2 bubbles is the reaction between Al and SO_3 that is contained in the soda-lime glass.

4. Conclusions

The corrosion behaviour of Fe-40Al-Zr in molten soda-lime glass has been studied at 1200 °C and the results were compared with previously tested alloys. The results can be summarized as follows:

1. The corrosion resistance of Fe-40Al-Zr alloy against molten soda-lime glass is lower compared to austenitic steel (EN X8CrNi25-21), because this alloy was dissolved faster and the surface of the sample is more disrupted.

2. The corrosion resistance of Fe-40Al-Zr is also lower than that of iron aluminide without Zr. It is obvious, that the presence of 0.09 % Zr reduces the corrosion resistance of iron aluminides against molten soda-lime glass as in the case of high-temperature oxidation of iron aluminides with Zr addition in air.

3. The corrosion mechanism of Fe-40Al-Zr alloy is characterized by the formation of alumina, FeSi and Fe_3Si. It seems that the saturation of molten glass by these products reduces further reaction between Fe-40Al-Zr alloy and the molten glass (unsaturated). The preferential oxidation of Zr was also observed. The preferential oxidation of Zr in particles causes a non-uniform attack of the sample surface and the increase of the oxidation rate.

Acknowledgements

The authors wish to thank P. Novák (Institute of Chemical Technology) for XRF analysis and P. Kejzlar (Technical University of Liberec) for EDS analyses. This work was supported by the Czech Science Foundation (GAČR P107/10/0438).

References

[1] McKamey, C. G., De Van, J. H., Tortorelli, P. F., Sikka, V. K. J.: Mater Res, *6*, 1991, p. 1779. doi:10.1557/JMR.1991.1779
[2] Tortorelli, P. F., Natesan, K.: Mat. Sci. Eng. A, *258*, 1998, p. 115. doi:10.1016/S0921-5093(98)00924-1
[3] Prescott, R., Graham, M. J.: Oxid Met, *38*, 1992, p. 73. doi:10.1007/BF00665045
[4] Risanti, D. D., Sauthoff, G.: Intermetallics, *13*, 2005, p. 1313. doi:10.1016/j.intermet.2004.12.029
[5] Palm, M., Sauthoff, G.: Intermetallics, *12*, 2004, p. 1345. doi:10.1016/j.intermet.2004.03.017
[6] Stein, F., Palm, M., Sauthoff, G.: Intermetallics, *13*, 2005, p. 1275. doi:10.1016/j.intermet.2004.08.013
[7] Milenkovic, S., Palm, M.: Intermetallics, *16*, 2008, p. 1212. doi:10.1016/j.intermet.2008.07.007
[8] Chevalier, S., Juzon, P., Borchardt, G., Galerie, A., Przybylski, K., Larpin, J. P.: Oxid Met, *73*, 2010, p. 43. doi:10.1007/s11085-009-9168-8
[9] Natesan, K.: Mat Sci Eng A, *258*, 1998, p. 126. doi:10.1016/S0921-5093(98)00925-3
[10] Pint, B. A., Tortorelli, P. F., Wright, I. G.: Mater High Temp, *16*, 1999, p. 1. doi:10.3184/096034099783641236
[11] Ni, J., Wan, X. J., Wang, Q., Cheng, X. Y., Liu, W. M., Zhang, X. Y.: J Shanghai Univ, *1*, 1997, p. 79. doi:10.1007/s11741-997-0049-6

[12] Janda, D., Galetz, M., Schütze, M., Heilmaier, M.: In: Proceedings of 6th Discussion Meeting on the Development of Innovative Iron Aluminium Alloys FEAL 2011. Eds.: Trujillo, F. J. P., Morris, D. G. Madrid, Spain, Department of Physical Metallurgy, CENIM-CSIC 2011, p. 133.
[13] Hotař, A., Palm, M., Kratochvíl, P., Vodičková, V., Daniš, S.: Corr. Sci., *63*, 2012, p. 71. doi:10.1016/j.corsci.2012.05.027
[14] Uxa, V.: Sklář a keramik, *6*, 1956, p. 225 (in Czech).
[15] Hotař, A., Kratochvíl, P.: Intermetallics, *15*, 2007, p. 439. doi:10.1016/j.intermet.2006.07.006
[16] Hotař, A., Kratochvíl, P., Hotař, V.: Kovove Mater., *47*, 2009, p. 247.
[17] Schindler, I., Kawulok, P., Fabík, R.: In: Proceedings of 2nd International Conference on Recent Trends in Structural Materials. Ostrava, Tanger Ltd. 2012. ISBN 978-80-87294-34-5, http://www.comat.cz/files/proceedings/11/reports/992.pdf
[18] Hotař, V., Novotný, F.: In: Proceedings of 11th International Conference on Fracture. Ed.: Carpinteri, A. Turin, CCI Centro Congressi Internazionale s.r.l 2005, p. 58.
[19] Mandelbrot, B. B.: The fractal geometry of nature. 2nd ed. New York, Freeman WH and Co. 1982.
[20] Peitgen, H. O., Juergens, H., Saupe, D.: Chaos and Fractals: New Frontiers of Science. New York, Berlin, Heidelberg, Springer-Verlag 1992. doi:10.1007/978-1-4757-4740-9
[21] Xu, C. H., Gao, W., Gong, H.: Intermetallics, *8*, 2000, p. 769. doi:10.1016/S0966-9795(00)00007-8